Supporting Information

Visualizing helical stacking of octahedral metallomesogens with chiral core

Go Watanabe*[a], Hideyo Watanabe,[b] Kota Suzuki,[b] Hidetaka Yuge,[b] Shintaro Yoshida,[a] Takuyoshi Mandai,[a] Shigetaka Yoneda,[a] Hisako Sato,[c] Mitsuo Hara,*[d] and Jun Yoshida*[b]

[a] Department of Physics, School of Science, Kitasato University, 1-15-1, Kitasato, Minami-ku, Sagamihara 252-0373, Japan

[b] Department of Chemistry, School of Science, Kitasato University, 1-15-1, Kitasato, Minami-ku, Sagamihara 252-0373, Japan.

[c] Department of Chemistry, Graduate School of Science and Engineering, Ehime University, 2-5, Bunkyo-cho, Matsuyama 790-8577, Japan.

[d] Department of Molecular and Macromolecular Chemistry, Graduate School of Engineering, Nagoya University, Furo-cho, Chikusa-ku, Nagoya, 464-8603, Japan.

Table of Contents

General information

Physical measurements

^{1}H NMR spectra were recorded at 600 MHz with a Bruker AVANCE-II-600. UV-Vis and electronic circular dichroism (ECD) spectra were recorded with V-570 and J-720 spectrometers (JASCO Corp.), respectively. Electrospray ionization (ESI) mass spectrometry was performed with an Exactive Plus (Thermo Fisher Scientific) spectrometer; the mass range was 20–2000 with a nominal resolution (at *m/z* 200) of 140,000. Elemental analyses were carried out using a Perkin Elmer 2400II elemental analyzer. Textures of liquid crystal samples were observed using a polarizing optical microscope (CX-31 or BX-53, Olympus Corp.) and a hot stage (Imoto Machinery). DSC measurements were performed with a DSCvesta (Rigaku Corp.). X-ray diffraction was performed on an X-ray diffractometer SmartLab SE equipped with a D/teX Ultra 250 1D detector (Rigaku Corp.) using Cu Kα radiation (λ = 0.154 nm). The samples were encapsulated into capillary tubes (ϕ = 0.5 mm) and the temperature was controlled with a PTC-EVO (Rigaku Corp.).

DFT calculation

The structural optimization of [Ru(acacC_2Ph)$_3$] (HacacC_2Ph = 3-(phenylethynyl)pentane-2,4-dione) was performed by DFT method using Gaussian 16[1] with ub3lyp functional. The 6-311G(d) basis set was employed for the C, H, and O atoms while LANL2DZ basis set[2–4] was used for the Ru atom with associated ECP. Ru atom was treated as an open shell doublet. The optimized structure was confirmed to be a minimum by frequency calculation. The calculated dipole moment is 0.92.

Sample preparation and optical resolution

Racemic **Ru-C8** was prepared via step-wise modification of [Ru(acac)$_3$] (acac=acetylacetonate) according to our previously reported procedure.[5] The spectroscopic data of the compound is as follows: Anal. Calcd (%) for $C_{111}H_{177}O_{15}Ru$: C 71.96, H 9.63; found: C 72.11, H 10.03. ^{1}H NMR (600 MHz, Chloroform-*d*) δ 3.79 (t, *J* = 6.5 Hz, 12H), 3.74 (t, *J* = 6.6 Hz, 6H), 3.32 (s, 6H), 1.74–1.61 (m, 18H), 1.44–1.33 (m, 18H), 1.33–1.17 (m, 72H), 0.92–0.81 (m, 27H), −6.37 (s, 18H). calculated for $C_{111}H_{177}O_{15}Ru$ ([M+H$^+$]) *m/z* = 1853.22, found 1853.22. The ^{1}H NMR spectrum of **Ru-C8** used in this study is shown in Fig. S1.

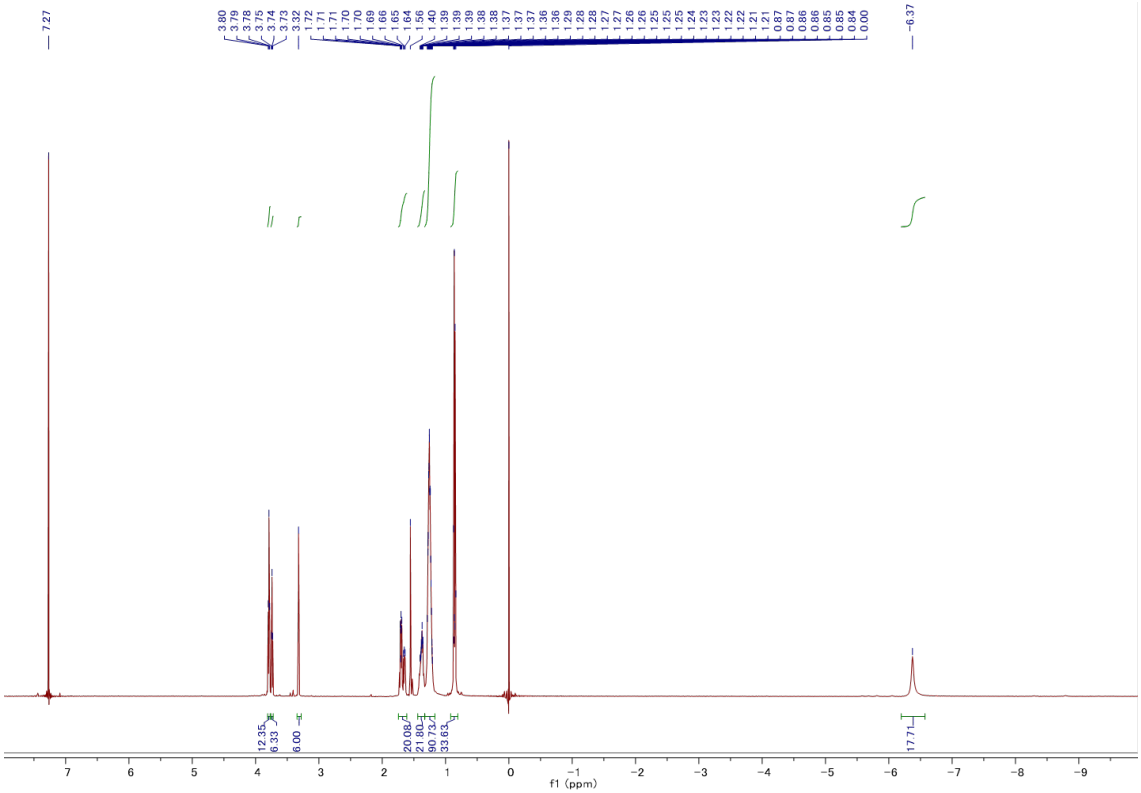

Fig. S1 ^{1}H NMR spectrum of **Ru-C8** measured in $CDCl_3$

The optical resolution of **Ru-C8** was performed using HPLC with a semi-preparative chiral column (Chiralpak IA, Daicel Chemical Industries Co., Ltd.) in the same condition reported by us (mobile phase: *n*-hexane/2-propanol = 20/1 (v/v), flow rate = 6 ml min^{-1}).[5] The obtained chromatograms are shown in Fig. S2.

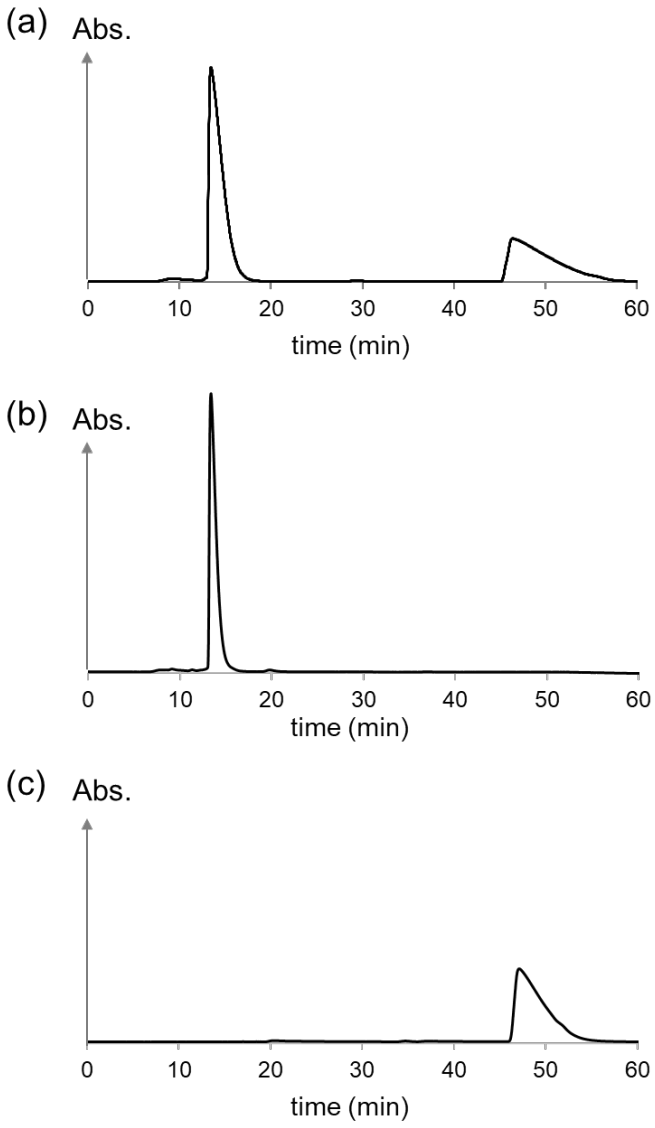

Fig. S2 (a) The HPLC chromatogram of *rac*-**Ru-C8** in a following condition; *n*-hexane/2-propanol = 20/1 (v/v), flow rate = 6 ml min^{-1}, detection at 360 nm. (b, c) The 1st and 2nd fractions in (a) were re-analyzed by HPLC to confirm the enantiopurity in the same chromatographic condition.

ESD spectroscopic studies

The less and more retained fractions were previously assigned as Λ and Δ isomers from ECD spectroscopy[5] by comparing the spectra with those of Δ, Λ-[Ru(acac)$_3$].[6,7] The ECD spectra are shown in Fig. S3(a). The optical isomers of **Ru-C8** were enantiomerically stable at least in the temperature range investigated in this study. ECD spectra of neat samples of Δ- and Λ-**Ru-C8** sandwiched between two quartz glasses were also measured (Fig. S3(b)). They show single positive and negative signals in the wavelength range of 400–550 nm, respectively, while those in solution show multiple Cotton effects in the same wavelength range. The large ECD signals observed for neat Δ- and Λ-**Ru-C8** samples are attributed to the formation of helical structures.

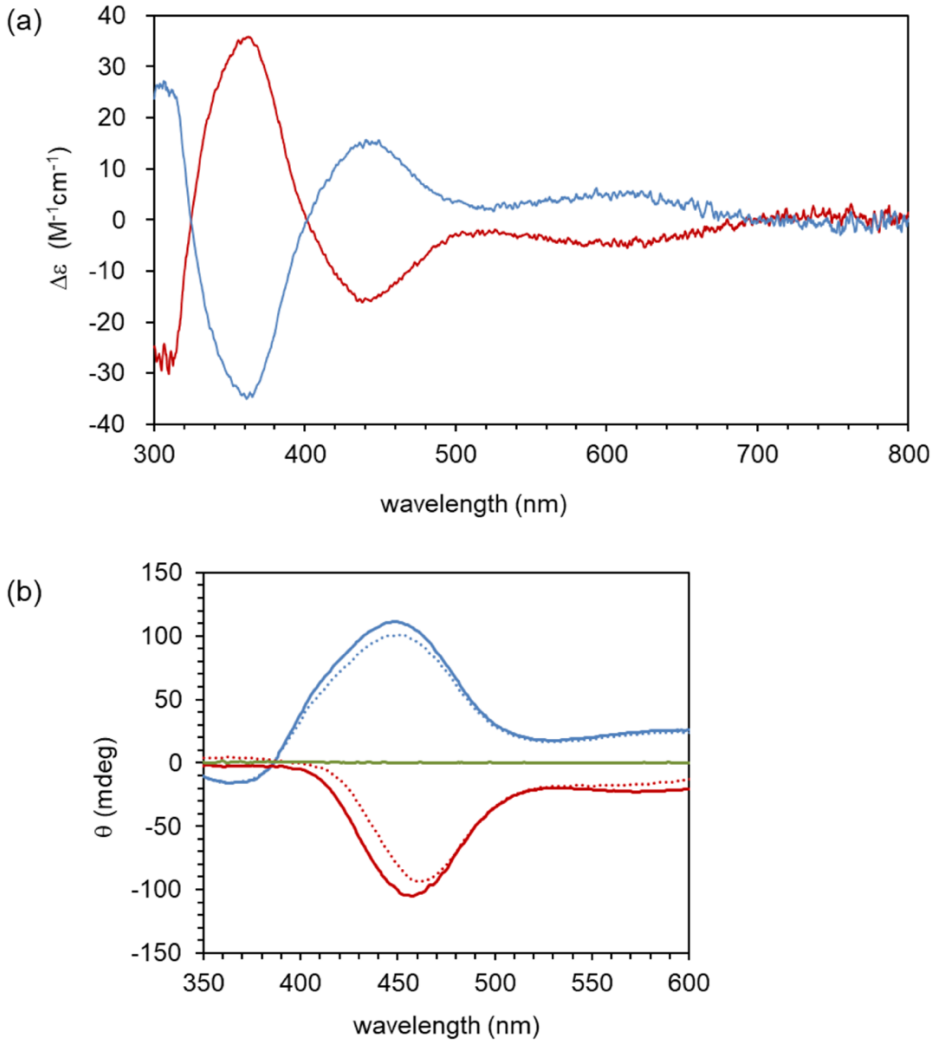

Fig. S3 (a) Solution ECD spectra of enantiopure **Ru-C8** measured in hexane. Red and blue lines correspond to Λ and Δ isomers, respectively. (b) Thin film ECD spectra of **Ru-C8** sandwiched between two quartz glass plates. Red, blue, and green lines correspond to Λ isomer, Δ isomer, and racemate respectively. The Λ and Δ isomers each were measured twice by rotating 90 degrees (dotted lines).

Characterization of phase behaviors

The phase behavior of enantiopure **Ru-C8** was also examined by DSC, POM, and XRD. On first heating with a rate of 10 °C/min, Δ-**Ru-C8** exhibits only one transition at 51 °C with an enthalpy of 7 J/g (Fig. S4). Upon subsequent cooling, broad endothermic peak was observed with the center at around 30 °C. Upon subsequent heating, additional small peak was observed at 25 °C in addition to the peak at 52 °C. The peak at 25 °C is attributed to melting (crystal-to-liquid crystal) transition, while the peak at 51 °C in the 1st scan is attributed to clearing (liquid crystal-to-isotropic) transition. Similar behavior was also observed for the Λ isomer. In the POM observation, enantiopure **Ru-C8** exhibited birefringent textures with microdomains upon annealing at 40 °C (Δ isomer: Fig. 2b in the main article, Λ isomer: Fig. S5). The enantiopure samples also showed little indication of crystallization in the POM observation at ambient temperature (Fig. S5(a)), while the time-course POM observation of Λ-**Ru-C8** confirmed that it partially crystalized very slowly over a month (for Λ-**Ru-C8** in Fig. S5(b)). The mesophase in enantiomers of **Ru-C8** was identified as a hexagonal columnar (Col_h) phase by the XRD measurement at 30 °C (Fig. 3a in the main article). The time-course XRD measurement at ambient temperature also confirms the slow crystallization (Fig. S6).

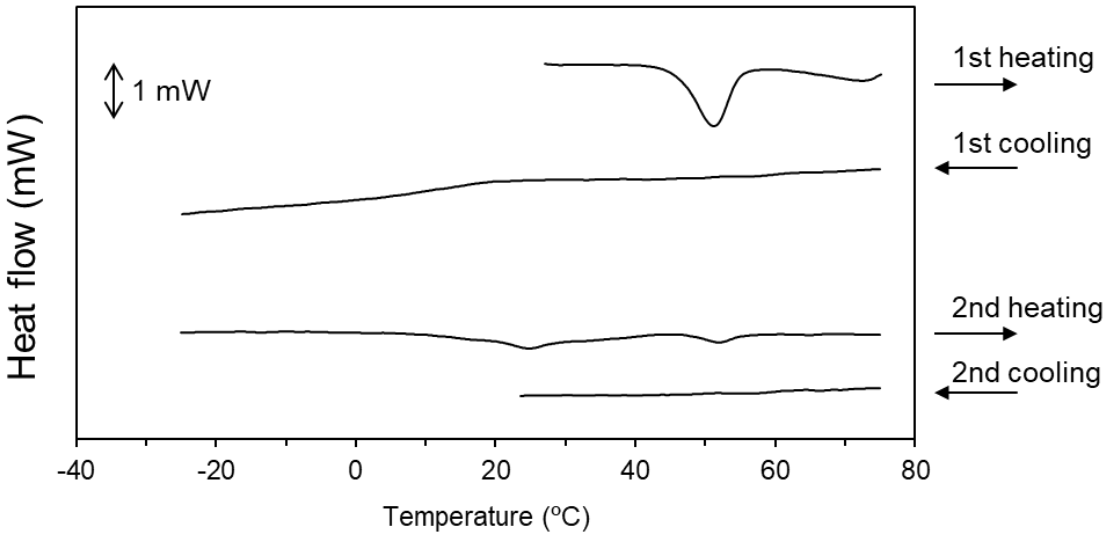

Fig. S4 The DSC traces of Δ–**Ru-C8** measured with the heating and cooling rates of 10 °C min^{-1}.

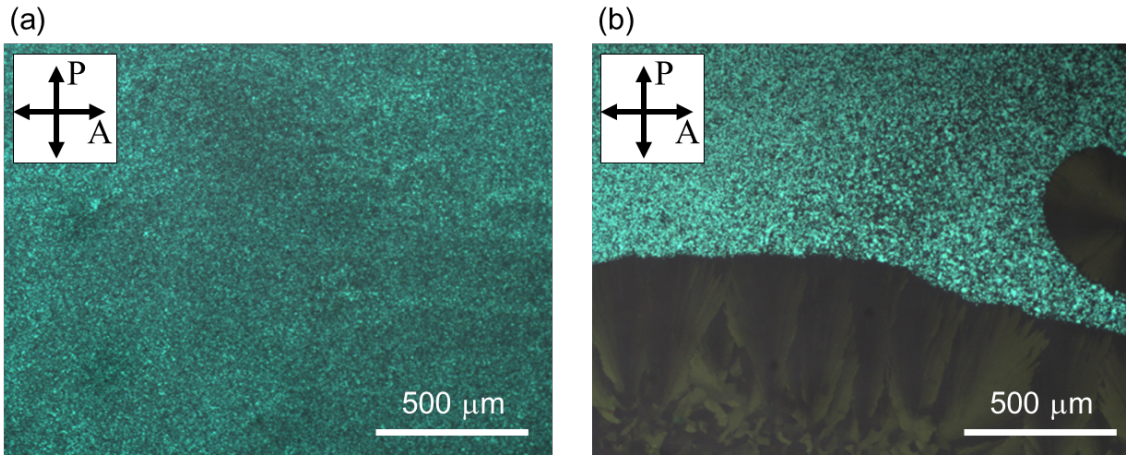

Fig. S5 Time-course POM observation of Λ-**Ru-C8** at ambient temperatures; the images were taken for the almost same region (a) soon after cooling from the isotropic state and (b) after the sample was kept at ambient temperature for a month. The bottom region in (b) indicates the crystallization of Λ-**Ru-C8**. The directions of the polarizer and analyzer are shown in the insets.

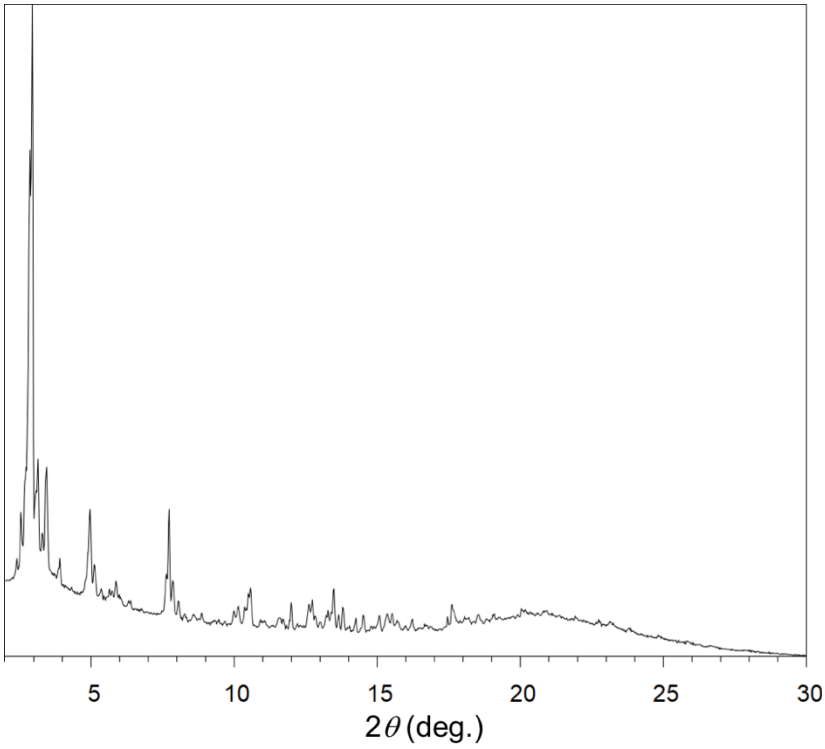

Fig. S6 XRD pattern of Δ-**Ru-C8** measured at ambient temperature. The metal complexes were injected in a capillary tube, heated to the isotropic state, and left at ambient temperature over a month before the measurement.

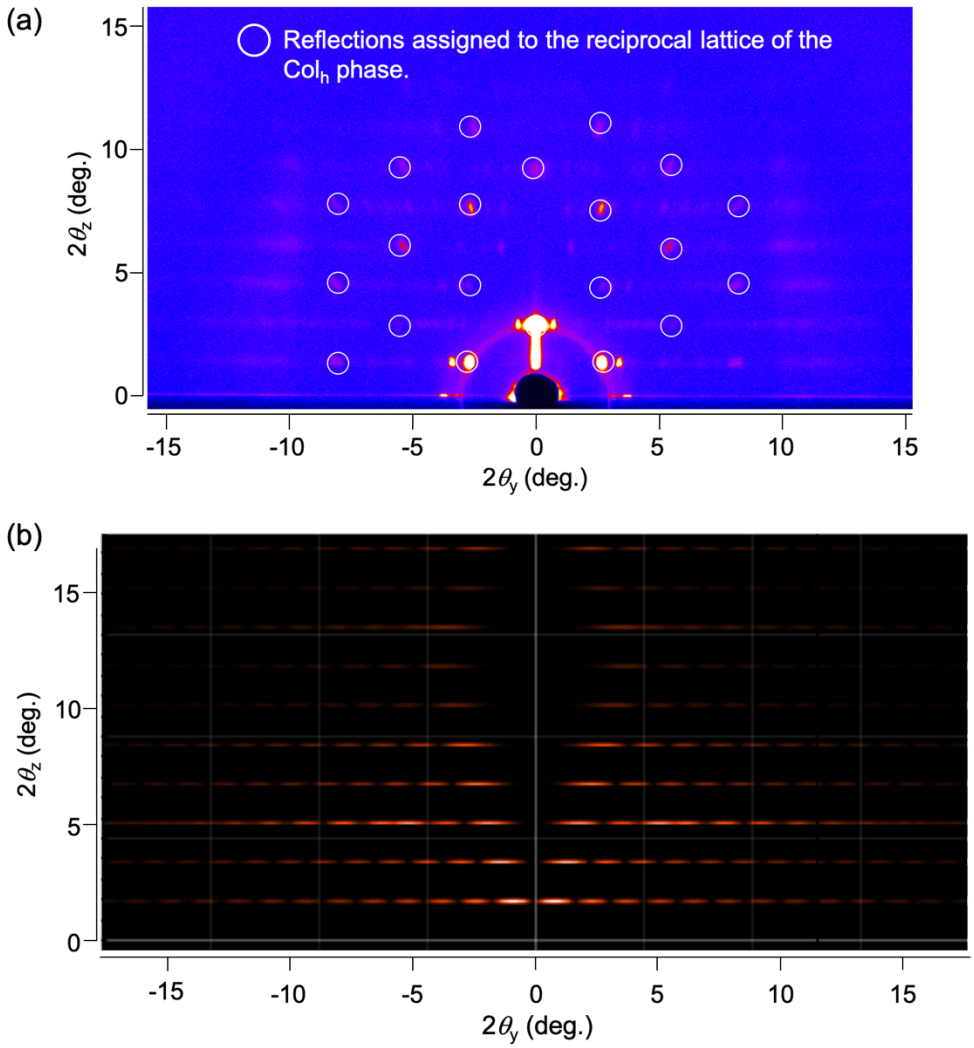

Fig. S7 (a) GI-XRD image of Δ-**Ru-C8** obtained at 37 °C. Reflections attributed to the reciprocal lattice of the Col$_h$ phase are circled in white. (b) Theoretical diffraction pattern simulated for a helix; helical pitch = 5.2 nm, units per a pitch = 14, and helix width = 3.2 nm. The simulation was performed by *Helical Diffraction Simulator* developed Stefan Huber (http://spring.embl.de/hspss/index.html), which was developed based on SPRING program.

GI-XRD measurements

Grazing-incidence X-ray diffraction (GI-XRD) was performed on an X-ray diffractometer FR-E equipped with a two-dimensional detector R-axis IV (Rigaku Corp.) involving an imaging plate (Fujifilm Corp.). X-ray from Cu Kα radiation (λ = 0.154 nm) was collimated to 0.3 mm, while the camera length was set at 300 mm. An incident angle of the beam to the substrate surface was adjusted at ca. 0.18−0.22° by using a Z pulse motor stage ALV-300-HM and an oblique pulse motor stage ATSC310-EM (Chuo Precision Industrial Co., Ltd.).

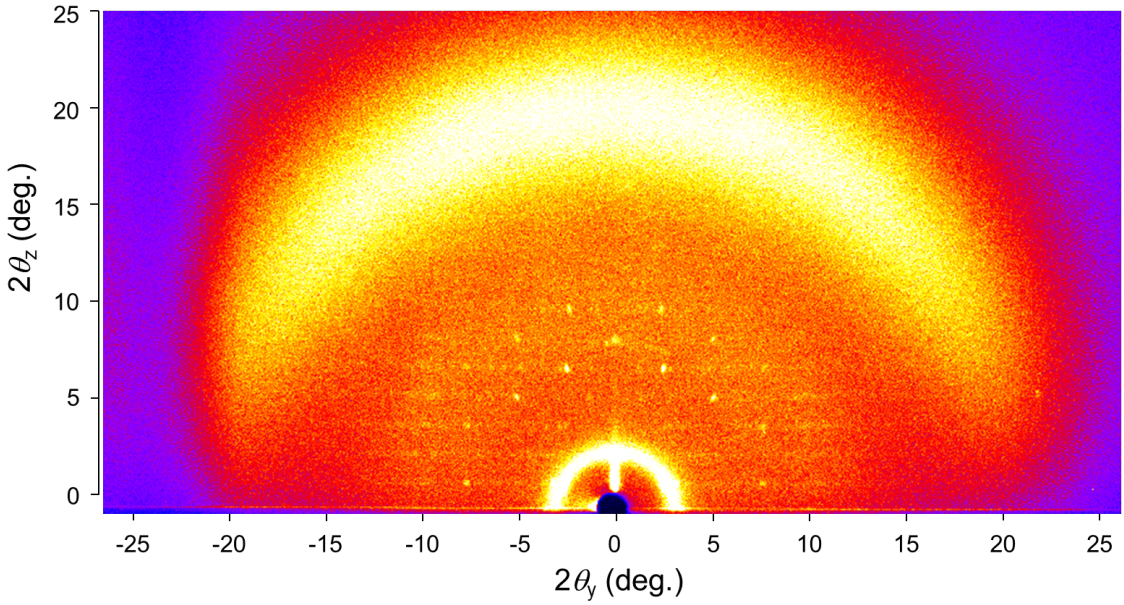

Fig. S8 The GI-XRD image of Λ-**Ru-C8** measured at 37 °C.

Molecular dynamics simulation

An all-atom model was used in accordance with generalized Amber force field parameters[8] in order to treat the intra- and interatomic interactions explicitly. The universal force field parameters were adopted as the parameters for the bond stretching and bond angle bending interactions, including the interatomic bonds between ruthenium and its neighboring oxygen atoms by referring the previous studies.[9,10] The partial atomic charges of Δ- and Λ-**Ru-C8** were obtained by using the restrained electrostatic potential (RESP) methodology, based on single point DFT calculations based on the Gaussian 09 program[11] with the B3LYP functional using 6-31G* basis set for the atoms, except ruthenium, for which the LANL2DZ basis set was used with the associated effective core potential.

The number of molecules in each system was 448 molecules. In the initial structure, 16 columns with two-fold helical pitches were positioned in the hexagonal lattice cell of dimensions 12.95 nm × 12.95 nm × 10.60 nm. For all MD simulations, the time step was set to 2 fs since all bonds connected to hydrogen atoms were constrained with the LINCS algorithm.[12] The smooth particle-mesh Ewald (PME) method was employed to treat the long-range electrostatic interactions. The real space cutoff and the grid spacing are 1.4 and 0.30 nm, respectively. The van der Waals interactions were calculated with the cutoff of 1.4 nm.

The initial relaxation runs were performed after the steepest descent energy minimization as follows: 10 ns at 250 K and 310 K, consecutively. During the relaxation runs, the Berendsen thermostat and barostat with relaxation times of 0.2 and 2.0 ps, respectively. Then, the equilibration run was carried out for 200 ns keeping at 310 K using the Nosé-Hoover thermostat[13] with relaxation time of 1.0 ps. The pressure of the system was kept under 1 bar using Parrinello-Rahman barostat[14] with relaxation time of 5.0 ps and the compressibility of 1.0×10^{-5} bar^{-1}. To obtain the reliable simulation results, all MD simulations in the present study were carried out with anisotropic pressure coupling. For *M*-Δ-**Ru-C8**, the hexagonal symmetry of the MD cell was maintained at the equilibrium state. The time dependencies of the six lattice parameters (*a*, *b*, *c*, α, β, and γ) are shown in Fig. S9-Fig. S14. It was also confirmed that the hexagonal MD cell was maintained for *P*-Δ-**Ru-C8** and *P*-Λ-**Ru-C8** after the 200 ns run.

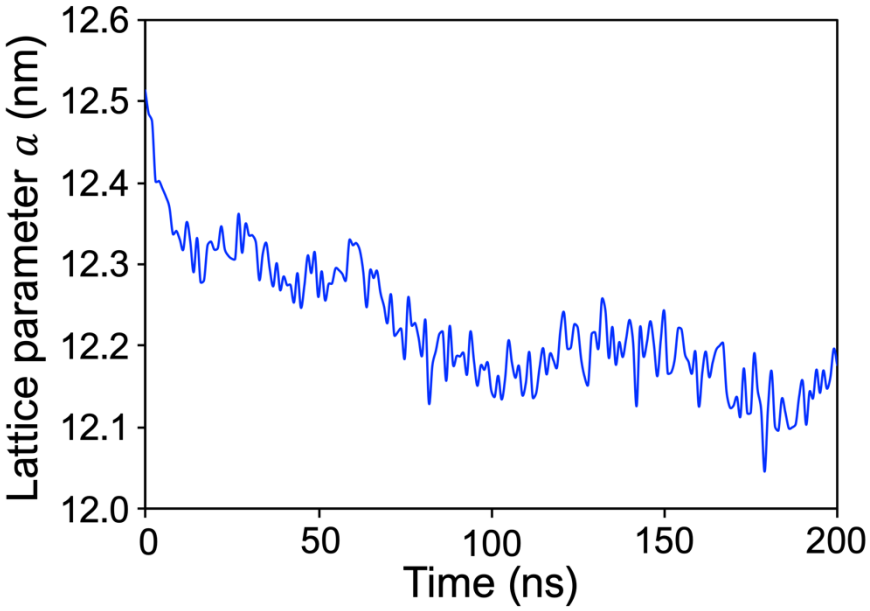

Fig. S9 Time dependence of the lattice parameter *a* of the hexagonal MD cell for *M*-Δ-**Ru-C8**.

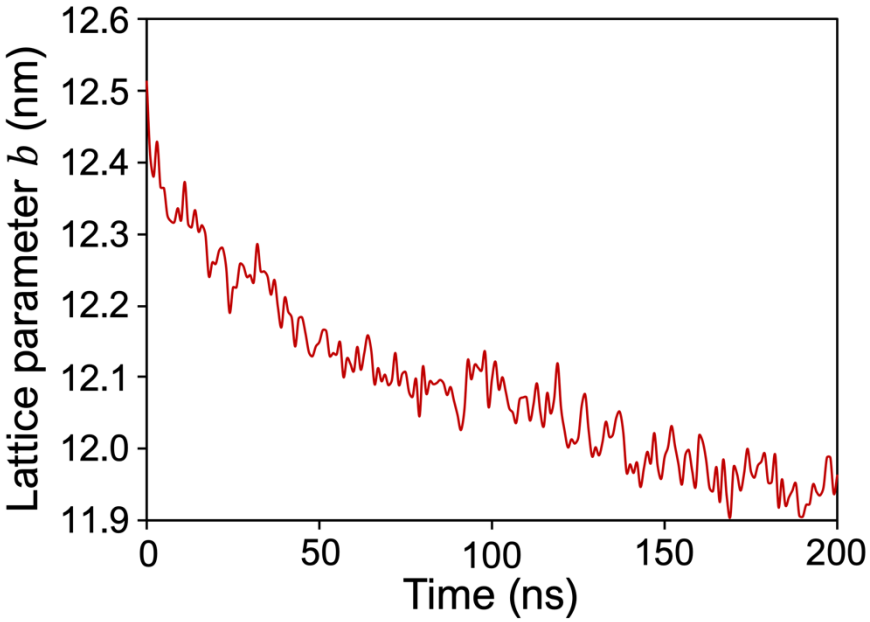

Fig. S10 Time dependence of the lattice parameter *b* of the hexagonal MD cell for *M*-Δ-**Ru-C8**.

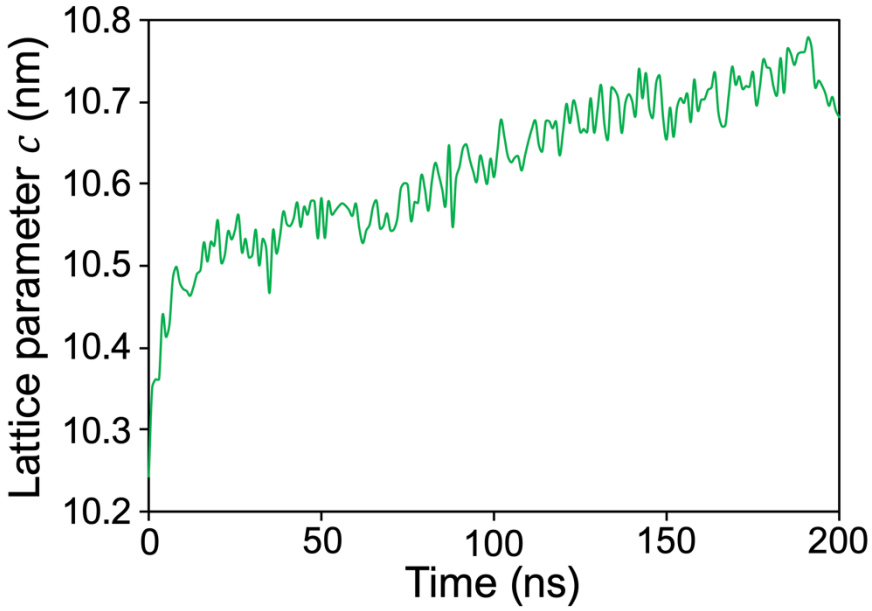

Fig. S11 Time dependence of the lattice parameter *c* of the hexagonal MD cell for *M*-Δ-**Ru-C8**.

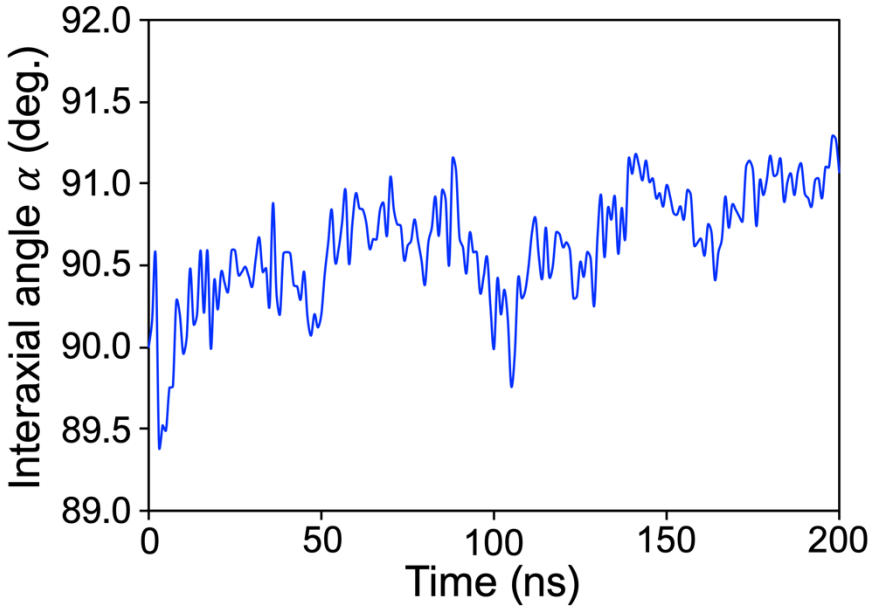

Fig. S12 Time dependence of the interaxial angle α of the hexagonal MD cell for *M*-Δ-**Ru-C8**.

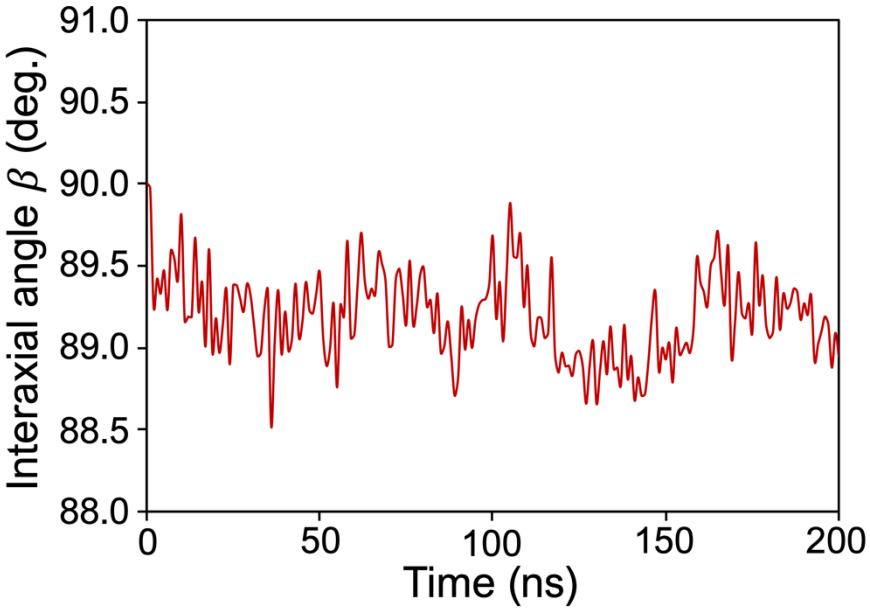

Fig. S13 Time dependence of the interaxial angle β of the hexagonal MD cell for *M*-Δ-**Ru-C8**.

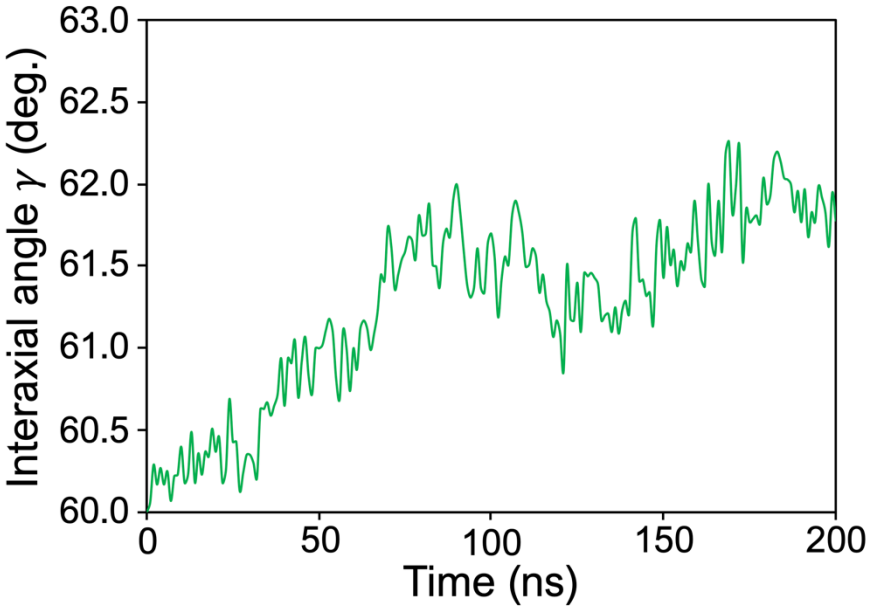

Fig. S14 Time dependence of the interaxial angle γ of the hexagonal MD cell for *M*-Δ-**Ru-C8**.

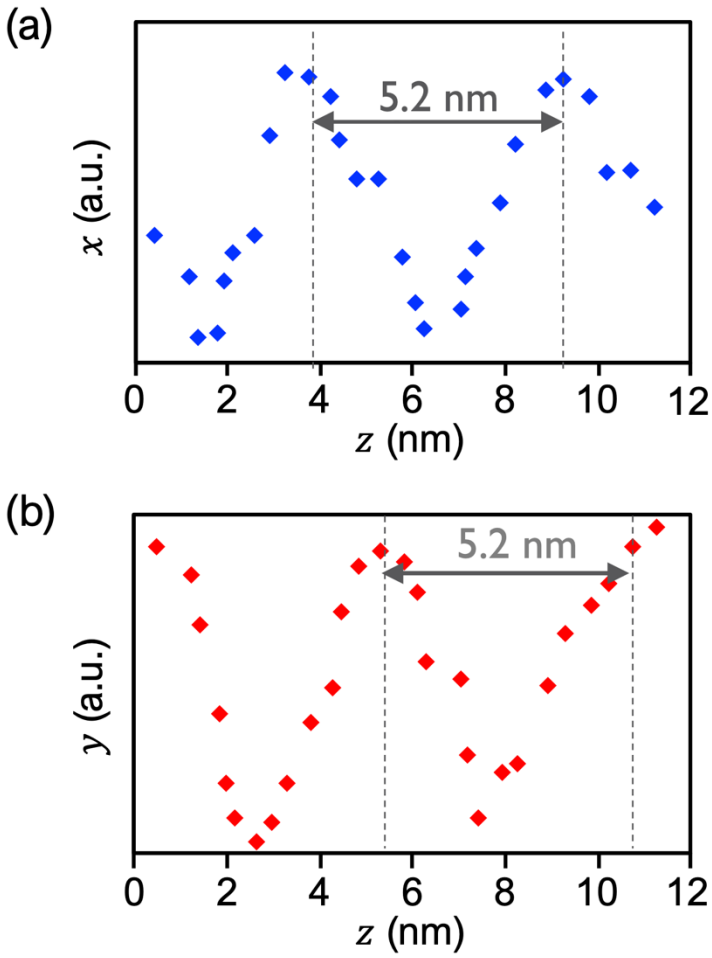

Fig. S15 (a) *z*-*x* and (b) *z*-*y* plots for the center of the mass of the molecules in a single column for *M*-Δ-**Ru-C8**.

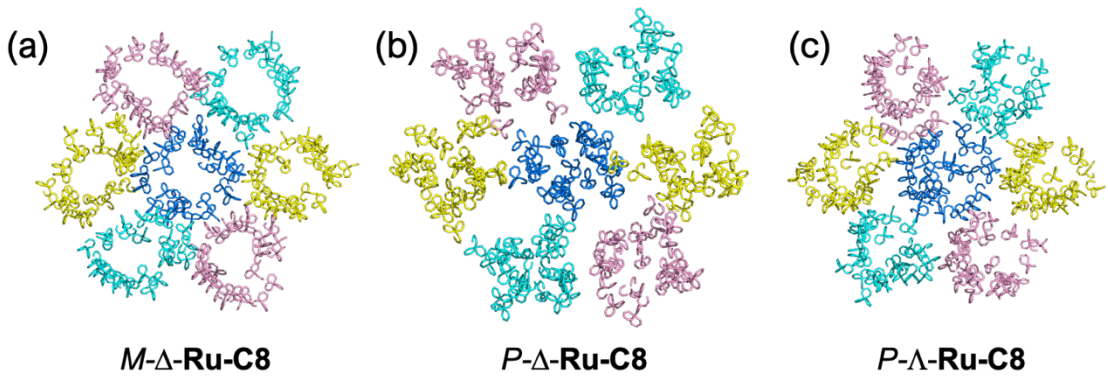

Fig. S16 Top view of stacked Ru cores (ruthenium and neighboring atoms) in 7 columns, which were extracted from 16 columns in the cell of the MD simulation snapshots at 200 ns: (a) *M*-Δ-**Ru-C8**, (b) *P*-Δ-**Ru-C8**, and (c) *P*-Λ-**Ru-C8**.

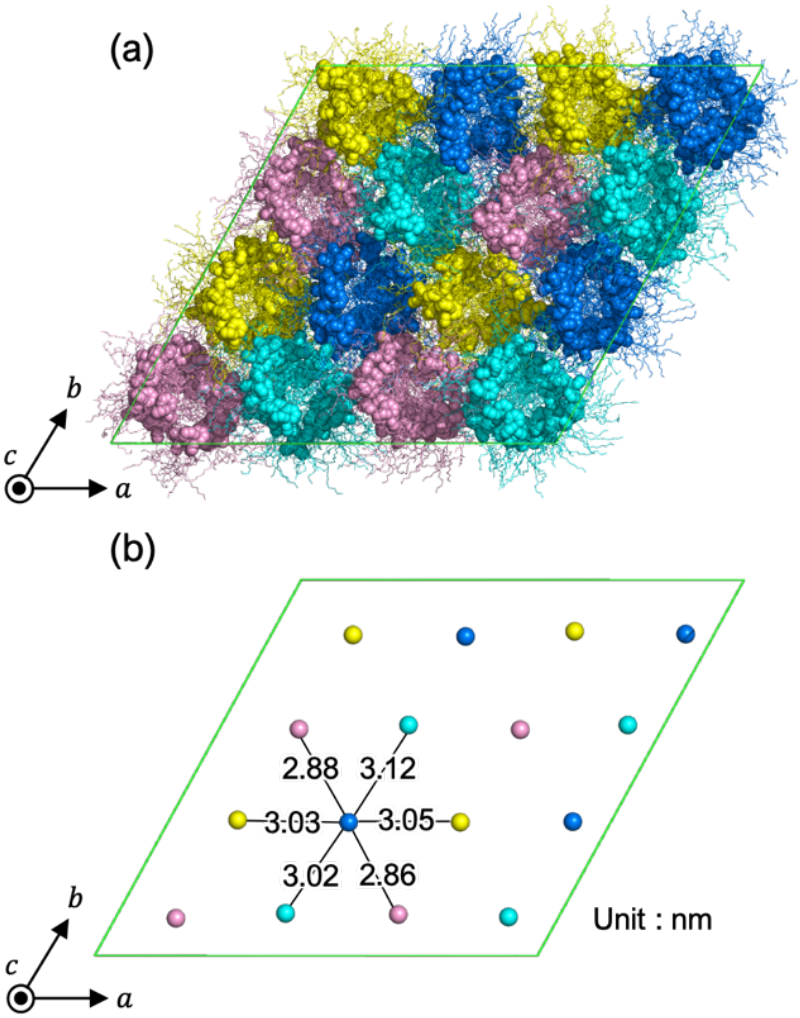

Fig. S17 (a) Top view of *P*-Λ-**Ru-C8** after 200 ns of MD simulation. The rigid core structure and peripheral group in each mesogen is represented by sphere and stick, respectively. (b) The average positions of Ru atoms in each column.

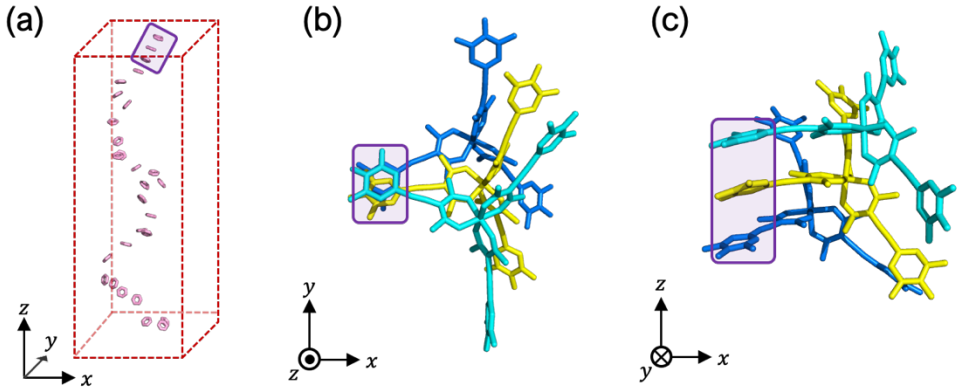

Fig. S18 (a) Phenylene rings of a single column in *M*-Δ-**Ru-C8** are only shown with three π-stacking ones highlighted with a violet rectangle. Three stacking Y-shaped molecules, involving the highlighted phenylene rings in (a), are shown along (b) the *z* axis and (c) the *y* axis (terminal alkyl chains were omitted for clarity).

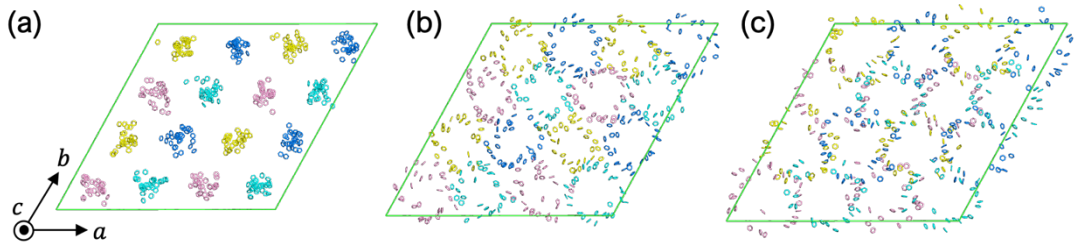

Fig. S19 The three phenylene groups in *P*-Λ-**Ru-C8** are shown separately for (a) those positioned at the interior of the helix, (b) near the Ru-core, and (c) exterior of the helix.

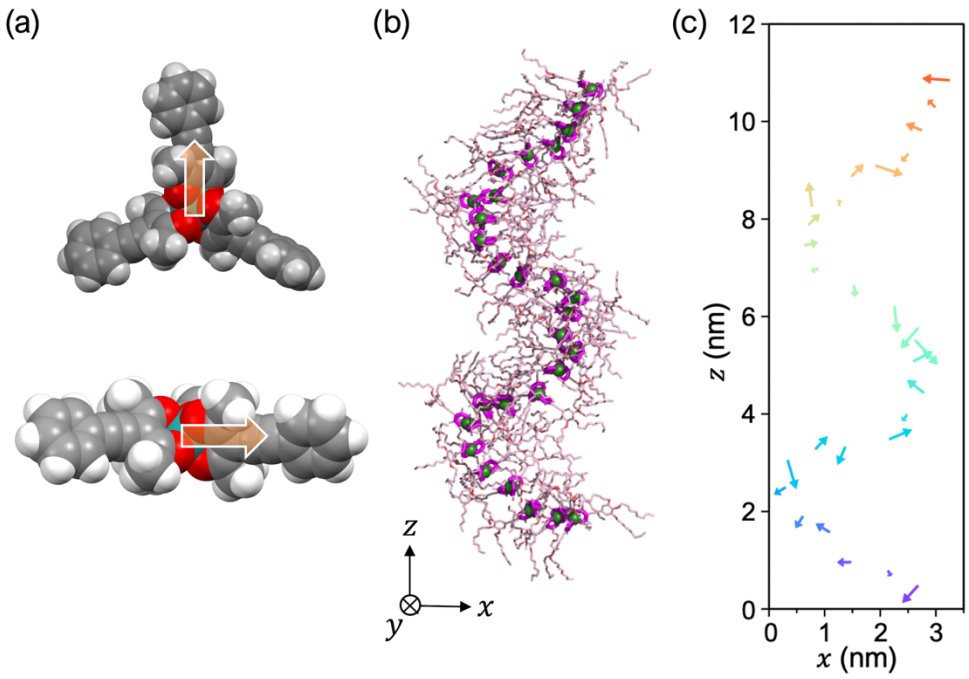

Fig. S20 (a) The DFT-optimized molecular structure of [Ru(acacC_2Ph)$_3$] with an overlay of calculated dipole moments (orange arrows). Distribution of dipole moments in a single column with a two-fold pitch obtained by MD simulation: (b) molecular coordinates used to calculate the dipole moments, (c) the projection of dipole moments on the *xz* plane.

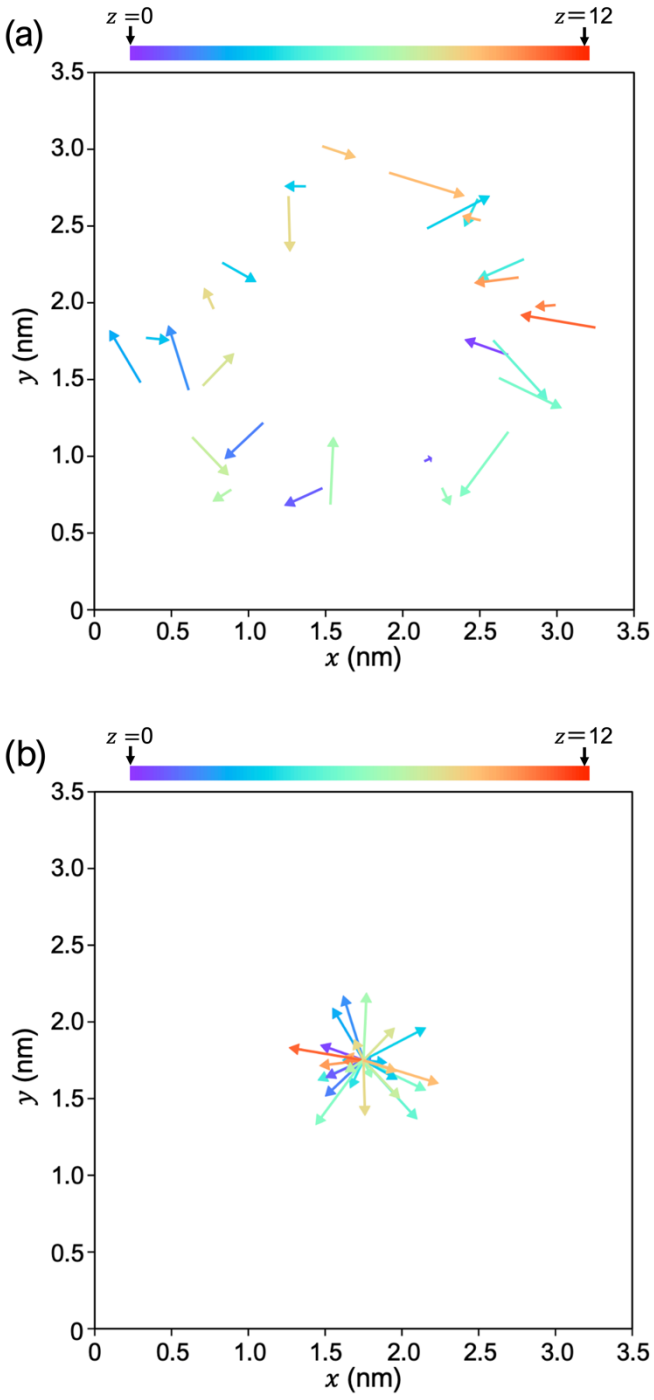

Fig. S21 The projection of dipole moments on the *x*-*y* plane in a single column with a two-fold pitch. The colors of the dipole moments correspond to the *z*-axis components. In (b), the starting point of all the dipole moments is set to the origin of the *xy* plane.

References

[1] M. J. Frisch, G. W. Trucks, H. B. Schlegel, G. E. Scuseria, M. A. Robb, J. R. Cheeseman, G. Scalmani, V. Barone, G. A. Petersson, H. Nakatsuji, et al., *Gaussian 16 (Revision C.01)*, Gaussian, Inc., Wallingford, 2016.

[2] P. J. Hay and W. R. Wadt, *J. Chem. Phys.,* 1985, **82**, 270–283.

[3] P. J. Hay and W. R. Wadt, *J. Chem. Phys.,* 1985, **82**, 299–310.

[4] W. R. Wadt and P. J. Hay, *J. Chem. Phys.,* 1985, **82**, 284–298.

[5] J. Yoshida, G. Watanabe, K. Kakizawa, Y. Kawabata and H. Yuge, *Inorg. Chem.,* 2013, **52**, 11042–11050.

[6] H. Kobayashi, H. Matsuzawa, Y. Kaizu and A. Ichida, *Inorg. Chem.,* 1987, **26**, 4318–4323.

[7] H. Matsuzawa, Y. Ohashi, Y. Kaizu and H. Kobayashi, *Inorg. Chem.,* 1988, **27**, 2981–2985.

[8] J. Wang, R. M. Wolf, J. W. Caldwell, P. A. Kollman and D. A. Case, *J. Comput. Chem.,* 2004, **25**, 1157–1174.

[9] G. Watanabe and J. Yoshida, *J. Phys. Chem. B,* 2016, **120**, 6858–6864.

[10] J. Yoshida, S. Tamura, K. Hoshino, H. Yuge, H. Sato, A. Yamazaki, S. Yoneda and G. Watanabe, *J. Phys. Chem. B,* 2018, **122**, 10615–10626.

[11] M. J. Frisch, G. W. Trucks, H. B. Schlegel, G. E. Scuseria, M. A. Robb, J. R. Cheeseman, G. Scalmani, V. Barone, B. Mennucci, G. A. Petersson, et al., *Gaussian 09 (Revision E.01), Gaussian Inc., Wallingford* 2009.

[12] B. Hess, H. Bekker, H. J. C. Berendsen and J. G. E. M. Fraaije, *J. Comput. Chem.,* 1997, **18**, 1463–1472.

[13] N. Shuichi, *Mol. Phys.,* 1984, **52**, 255–268.

[14] M. Parrinello and A. Rahman, *J. Appl. Phys.,* 1981, **52**, 7182–7190.